Alumina-Hydroxyapatite-Silver Spheres With Antibacterial Activity

Pamela Nair Silva-Holguín[1] and Simón Yobanny Reyes-López[1] ⦿

Abstract

Researchers are currently looking for materials that are stable, functional, aesthetic, and biocompatible without infections. Therefore, there is a great interest in obtaining a material that has a balance between aesthetic, biological, mechanical, and functional factors, which can be used as an infection control material. The addition of hydroxyapatite to alumina make highly bioactive scaffolds with mechanical strength. Biomedical applications require antibacterial properties; therefore, this idea leads to great interest in the development of new synthetic routes of ceramic biomaterials that allow the release of nanoparticles or metal ions. This investigation presents the obtention of alumina-hydroxyapatite spheres doped with silver nanoparticles with antibacterial effect against various Gram-positive and negative bacteria related to drug-resistance infections. The microstructural and spectroscopic studies demonstrate that the spheres exhibit a homogeneous structure and crystal hydroxyapatite and silver nanoparticles are observed on the surface. The antimicrobial susceptibility was verified with the agar diffusion and turbidimetry methods in Gram-negative (*Escherichia coli* and *Pseudomonas aeruginosa*) and Gram-positive (*Staphylococcus aureus* and *Bacillus subtilis*) bacteria. All bacteria used were susceptible to the alumina-hydroxyapatite-silver spheres even at lower silver concentration. The composites have a higher possibility for medical applications focused on the control of drug-resistance microorganisms.

Introduction

The drug resistance by a variety of viruses, fungi and bacteria have increased dramatically in recent years generating serious health problems, therefore, we need to develop new materials with higher antimicrobial properties.[1] Resistance to antimicrobial agents is not a new phenomenon, for decades bacteria have developed special resistance systems against antibiotics, its mechanisms include: over expression of outflow pumps, metabolic pathways alternate to those inhibited by the drug, decrease bacterial cell wall permeability, degradation of the antibiotic, enzymatic modification of the antibiotic, modification of antibiotic targets, overproduction of the target enzyme and transfer of resistance genes.[2]

Currently, numerous infections with pathogenic microorganisms are becoming increasingly resistant to antibiotics, becoming a critical health problem.[3] For example: the high incidence of bacteria resistant to antibiotics, coupled with the prevalence of dental caries, has motivated the use of alternative antimicrobial agents based on metallic nanoparticles or their oxides. Under physiological conditions there is a symbiotic relationship between multiple species of non-pathogenic bacteria with the human oral cavity, where the commensal species by forming biofilms on the dental surface do not allow the adherence of pathogenic bacteria. A biofilm is an associate of bacterial species that adhere to a watery surface where there is the presence of nutrients. Within the great diversity that can exist in a biofilm, a minimal percentage may be involved potentially pathogenic bacteria, which due to an alteration in the oral ecosystem can cause disease.[4,5]

Dental cavities are a demineralization process that deteriorates and/or destroys the tissues of the teeth due to the presence of acids derived from the bacterial metabolism that occurs on dental surfaces. Within the pathogenesis of dental caries, the

[1] Instituto de Ciencias Biomédicas, Universidad Autónoma de Ciudad Juárez, Ciudad Juárez, Chihuahua, México

Corresponding Author:
Simón Yobanny Reyes-López, Instituto de Ciencias Biomédicas, Universidad Autónoma de Ciudad Juárez, Envolvente del PRONAF y Estocolmo s/n, Ciudad Juárez, Chihuahua, CP 32300, México.
Email: simon.reyes@uacj.mx

main associated microorganisms are *Streptococcus mutants*, *Lactobacillus spp* and *Actinomyces spp*, the most important is *Streptococcus mutans*, this microorganism could generate various acids (lactic acid, propionic acid, acetic acid and formic acid) derived from their metabolism of carbohydrates, which, when found in the medium, dissociate and release hydrogen ions. These chemical species can produce the release of calcium and phosphorus from the enamel by dissolving their mineral, thus causing demineralization.[4,6,7]

The oral cavity is the entrance to multiple microorganisms and possible infections in the gastrointestinal system and the respiratory system, it is necessary to consider other microorganisms. *Escherichia coli* is a Gram-negative bacterium that belongs to the intestinal microbiota, representing one of the most abundant species in the environment and establishing a symbiotic relationship. However, there are pathogenic strains that can cause infection, for example enteropathogenic *E. coli* is one of the most common causes of childhood diarrhea, because it induces the degeneration of microvilli in the intestine.[8] *Pseudomonas aeruginosa* is a Gram-negative bacterium that represents one of the most isolated species from the respiratory tract in seriously hospitalized patients, causing infections with high mortality due to high resistance to antibiotics.[9,10] *Staphylococcus aureus* is a Gram-positive bacterium that causes a wide variety of infections, mainly infections in the bloodstream and food poisoning, its main impact is due to strains resistant to methicillin (MRSA).[11]

Ceramic compounds are considered as third generation orthopedic biomaterials due to their ease of matching the chemical, biological and mechanical properties of bone. These types of materials are intended to support and stimulate tissue regeneration. Hydroxyapatite (HAp) is the main mineral component of human bone and dentin. Synthetic hydroxyapatite is commonly used in artificial prostheses because it has comparable chemical similarity to the mineral human skeleton. HAp has exceptional biocompatibility, high bioactivity, osteoconductive and chemical stability, but lacks mechanical strength, therefore, it is mixed with ceramic or polymer to form composite materials based on HAp with higher mechanical properties. Hydroxyapatite shows a low antibacterial property leading to research focused on enhancing its characteristic by doping or modifying its structure with bactericidal ions like Al, Fe, Ni, Pt, Ti, Sr, Zn, Ce, Au, Cu and Ag.[12-15]

For centuries, silver has been used to prevent and treat a wide variety of infections, but its use has decreased due to the discovery and innovation of a wide range of antibiotics, however, resistance caused by abuse of various antibiotics has renewed the interest in the use of silver in infection control.[16] The search for novel biomaterials should also include antibacterial properties. The ceramic-metal restorations are the basis of the current model of dentures, but despite their achievement, there are continued efforts to achieve more aesthetic, biocompatible, and bactericidal ceramic systems.[17] Ceramic materials are the best to imitate the natural appearance of the teeth. Ceramics based on alumina (Al_2O_3) have been recognized as materials for dentures and are required to be bioinert, have high

hardness and abrasion resistance.[18] Reinforcement of hydroxyapatite with metal oxide ceramics such as alumina (Al) enhance the mechanical stability and apatite formation. Several methods have been employed to synthesis HAp and Al composites such as sol-gel, coprecipitation, ball mill, microwave route, emulsion system and hydrothermal synthesis.[19] Chemical synthesis by precipitation and sol-gel are the experimental methods that are mostly used. Different reinforcing agents of metal oxides like titania, zirconia, silica and alumina in different scale (nanometric or submicrometric) and form like nanopowders, nanotubes, whiskers, platelets or fibers have been employed to improve the mechanical properties of HAp.[19,20] The nanocrystalline alumina is bioactive and conventional polycrystalline form is bioinert. Therefore, obtaining alumina and hydroxyapatite composites are attractive for use in implants. Alumina has been used in orthopedics application because of their excellent resistance to wear. However, when this oxide is used as a reinforcing agent for HAp, the decomposition of HA to β-TCP occurs dramatically, resulting in low densification and poor mechanical properties. In addition, interfacial reactions taking place in high temperature processing method limit the formation of pure phase. Therefore, efforts must be made to produce compounds entirely of Al_2O_3 and HAp; without HAp decomposition.[21]

Alumina structures have better mechanical resistance; however, due to a lack of appropriate cellular responses, they cannot interact with natural tissue. The application of alumina in the medical field plays an important role either from large prothesis to nanoparticles. Few studies are available in the literature about the interaction of the alumina bacterial species.[22-24] The possibility of adding the osteointegration properties of hydroxyapatite in alumina will give a material with mechanical and biocompatible properties. The search for novel biomaterials should also include antibacterial properties. Based on literature no experimental procedure on the preparation of Al_2O_3-HAp spheres composites with its antimicrobial properties has been reported. Metallic nanomaterials have attracted attention in the field of treatment of infections due to its ability to overcome bacterial resistance in contrast to existing antibiotics, because of the smaller particle size that cause greater damage even with a lower concentration.

It is known that metal nanoparticles or their oxides improve the antimicrobial power of composites. Research on the antimicrobial power of Ag nanoparticles (AgNPs) have contributed to the development of new materials with bacterial activity. The toxicity of silver nanoparticles is related and is dependent on various factors such as their size, shape, exposure time, reactivity, dissolution and release capacity of silver ions, but it is mainly dose dependent. In this investigation, a spherical alumina matrix material is manufactured for its hardness and support, then coated with hydroxyapatite to reproduce the appearance and composition of a tooth, to achieve 2 important characteristics: mechanical resistance and biocompatibility. In addition, the material is doped with silver nanoparticles to provide antimicrobial activity, seeking a balance between its aesthetic, functional, biological and mechanical property,
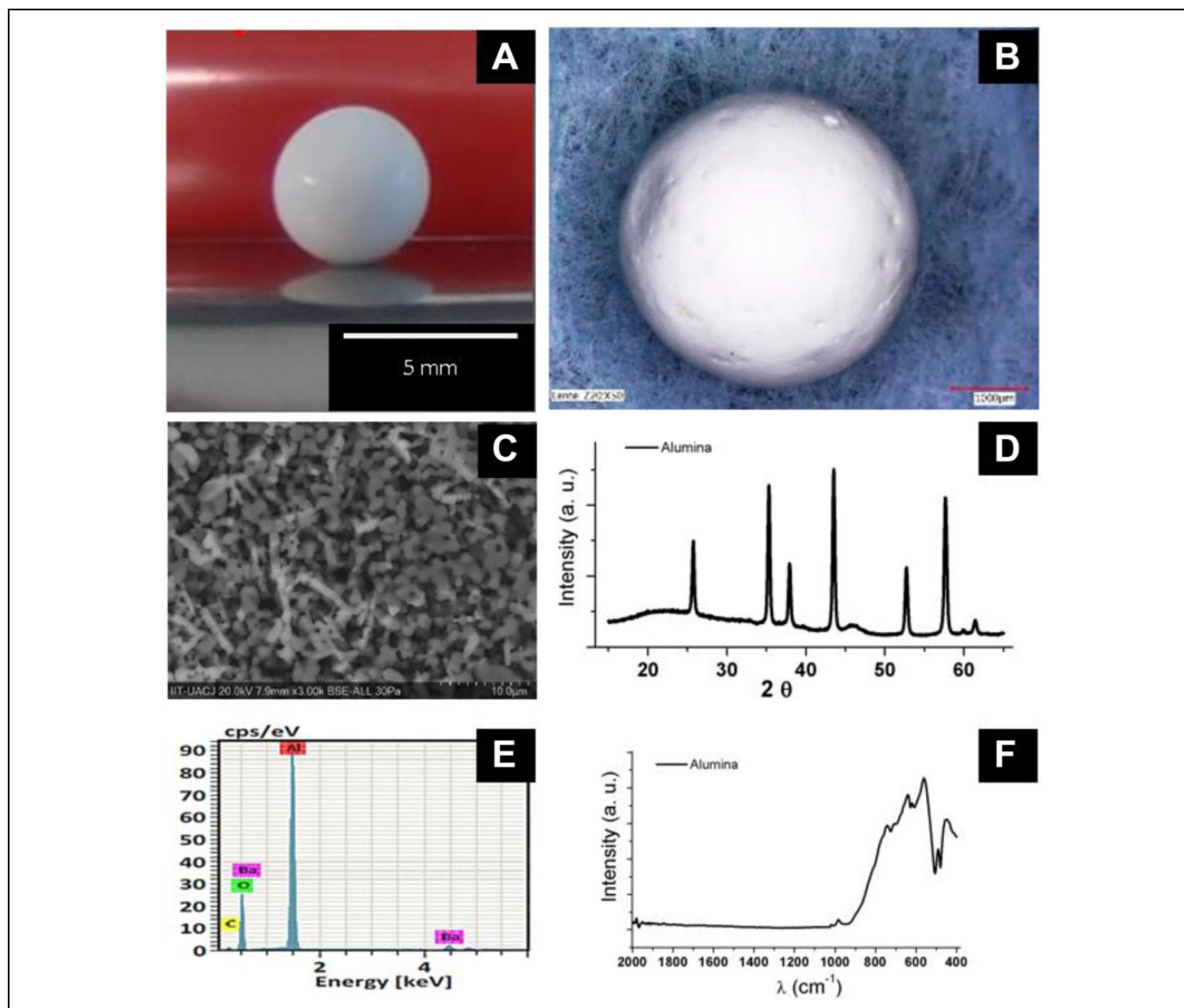
Figure 1. (A) Green spheres of alumina, (B) digital micrograph image, (C) SEM image, (D) XRD pattern, (E) EDX and (F) infrared spectra of alumina spheres at 1600°C.

resulting in a new material for use in controlling infections in the dental industry. The Al_2O_3-HAp-AgNPs composite was then evaluated against Gram-positive and negative bacteria related to drug-resistance infections at low concentration of silver to resolve to control microorganisms of clinical importance.

Materials and Methods

Preparation of Alumina-Hydroxyapatite-Silver Spheres (Al-HAp-AgNPs)

Alumina spheres: First, the alumina spheres were obtained using alginate as a template. Using a simple and inexpensive way to produce spherical beads. The encapsulation reaction occurs due to ion exchange, it starts when sodium alginate replaces its monovalent Na^+ ions by divalent Ca^{2+} ions to form a semi-rigid body. The use of a binder such as polyvinyl alcohol (PVA) is also required, which helps to bind particles heterogeneously, causing greater bonding between particles by capillary forces during the drying and sintering process.[23,25]

A mixture of alumina powder (1-3 μm, 99.99% Sigma Aldrich), deionized water, sodium alginate and PVA at 55%, 30%, 10% and 5% relation were used for formation of slurry. Alumina powder, PVA, sodium alginate and distilled water were stirred magnetically until a homogenous white slurry was obtained. The mixture was dropped dropwise onto the barium chloride solution ($BaCl_2$ 0.6 M). The spheres were left to age in the barium chloride for 24 h, after the time elapsed, they were placed in the oven at 100°C for 24 h, after 800°C for 2 h with a
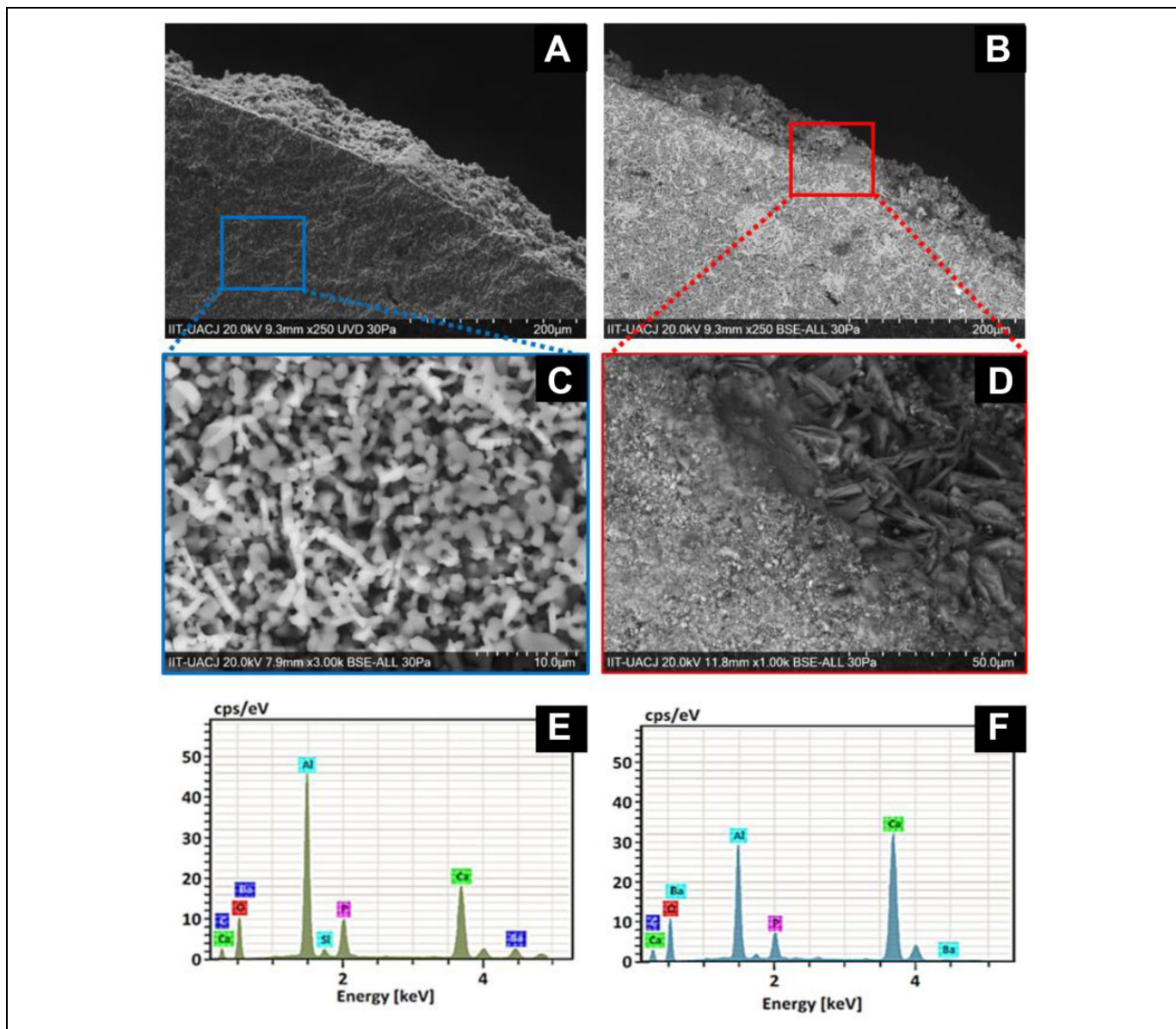
Figure 2. SEM micrographs of alumina-HAp sphere: (A) center of sphere, (B) surface, (C) center amplification for alumina, (D) surface amplification for HAp, (E) EDX center of sphere and (F) surface.

ramp of 5°C/min, finally, they were sintered at a temperature of 1600°C for 2 h with a ramp of 5°C/min. Second step involve coating the alumina spheres with hydroxyapatite.

Alumina-hydroxyapatite spheres (Al-HAp): Calcium nitrate tetrahydrate (Ca(NO$_3$)$_2$.4H$_2$O, CaN), triethyl phosphite ((C$_2$H$_5$O)$_3$P, P(OEt)$_3$) and ethanol were used as raw materials for the synthetized sol, all chemicals were obtained from Sigma-Aldrich Co. This synthesis was carried out by employing the method reported previously by Garibay-Alvarado et al in 2017.[26] The CaN was dissolved, and the P(OEt)$_3$ was hydrolyzed in ethanol. The CaN solution was added by dripping it into the triethyl phosphite with continous stirring for 24 h at 40°C 1 h, after some time, the temperature was increased to 60°C for 24 h under constant stirring to form a viscous white

sol-gel solution. The alumina spheres were immersed in the hydroxyapatite sol-gel solution to form the coating and allowed to dry at 100°C for 24 h, then they were placed in the muffle furnace at 970°C for 3 h with a ramp of 5°C/min to remove organic material and crystallize HA, this process was repeated in triplicate for further HA deposition.

Silver nanoparticles (AgNPs): The AgNPs was obtained by chemical reduction, in which silver nitrate was used as the metallic precursor, gallic acid as the reducing agent and sodium hydroxide as the stabilizing agent. In a 10 mM silver nitrate solution the reducing agent was added and immediately, afterward sodium hydroxide (1 M) was added dropwise to a pH of 11 to complete the reaction and stabilize the nanoparticles according to previous work.[27]
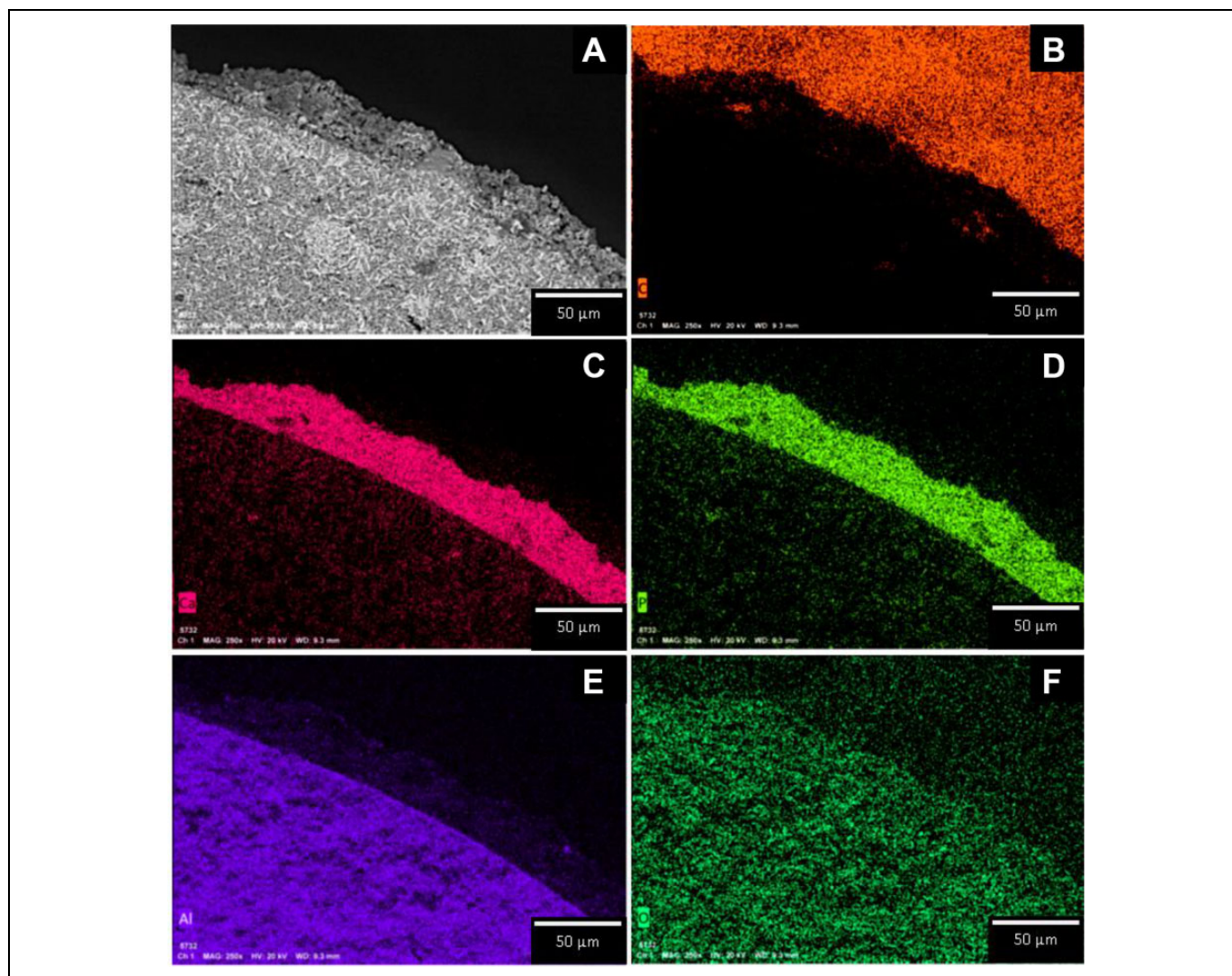
Figure 3. Compositional analysis EDX_SEM of alumina-hydroxyapatite sphere: (A) micrograph on secondary electrons, (B) carbon, (C) calcium, (D) phosphorus, (E) aluminum and (F) oxygen.

Alumina-hydroxyapatite-Ag spheres (Al-HAp-AgNPs): The final step in obtaining the silver spheres, was doping by a simple adsorption. The 10 mM silver nanoparticle solution was used, where the alumina-HAp spheres were immersed for 72 h. After the 72 h, the spheres were removed from the AgNPs solution and placed in the oven at 100°C for 24 h, then at 200°C for 3 h with a ramp of 5°C/min to remove water moisture.

Characterization

Vibrational bands of bonds and functional groups present in samples were determined by Fourier Transformed Infrared Spectroscopy (FTIR) and Raman. FTIR was carried out using a Bruker Alpha Platinum ATR spectrometer getting 48 scans per sample with a resolution of 4 cm^{-1} in a spectral range from 4000 to 400 cm^{-1}. Using a Raman Confocal alpha300 WiTec spectrometer, an integration time of 0.5 seconds, 10

accumulations and a 532 nm excitation laser source the characterization of the composites was carried. The composites were placed over carbon tape on a slide for its microstructural analysis, which was made in a Field Emission Scanning Electron microscope SU5000 Hitachi with an energy of 20 keV, an Energy Dispersive X-ray Spectroscopy (EDS) assay was carried out to know the elemental composition. Spheres were analyzed by the powder diffraction technique, in instrument X'Pert PRO PANalytical, with Cu kα = 1.54, 20 kV, in the range of 2θ of 10 to 80°, a 2°/min scanning speed. UV-Vis spectra were evaluated at 25°C in a Cary100 spectrophotometer (Varian Corp.) using a 10 mm quartz cell. Particle size and distribution were calculated by dynamic light scattering (DLS) in a Nanoparticle Analyzer SZ-100 (HORIBA).

Microstructural optical microanalysis was performed on a Keyence VHS 5000 brand digital microscope using a 50, 100 and 200× objective. For the observation of the phases of the sphere, an inverted metallographic microscope was used

Infinity 1 eclipse brand and a metallographic preparation was made, the sphere of alumina, alumina-hydroxyapatite and alumina-hydroxyapatite-AgNPs were encapsulated with epoxy resin and hardener brand LECO, once the resin hardened, the sample was roughly cut to the middle of the sphere. For roughing, a Struers LaboPol-35 brand polishing machine and LECO brand sandpaper with 400 to 1200 grain size were used, followed by mirror polishing with 3 and 1 μm diamond solution. To measure the compression force of the spheres, a Tinius Olsen Mod.h5oks brand tension machine was used with a test speed of 10 mm/min.

Antibacterial Activity

Disc diffusion method was performed to measure the antibacterial activity of Al-HAp-AgNPs compounds against *E. coli*, *P. aeruginosa*, *S. aureus* and *B. subtilis*. Microbial species were cultivated in soy broth for 20 h at 37°C, according to the McFarland scale (1.3×10^6 CFU/mL), 100 μL of standardized suspensions of each bacterium were placed on Müller-Hinton agar plates. 0.05 g of the spheres were considered for the antimicrobial activity study. Antibacterial tests were carried out by adapting the disk diffusion method using the suspension of bacteria spread on a Mueller-Hinton agar plate. The inoculated plates were incubated for 24 h at 37°C. The antibacterial effect was determined by measuring clear areas resulting from the inhibition formed around the compounds.[28] All tests for each microorganism were done in triplicate.

Minimum inhibitory concentration (MIC) was determined using the microbroth dilution method in a Multiskan MCC Fisher Scientific microplate reader. The procedure for evaluating the antimicrobial effect of the different samples was based on the same Gram-positive and Gram-negative bacterial culture. For the turbidimetry method, the test was performed in a 96-well microplate where 200 μL of the standardized inoculum of each bacterium and 5 mg of each treatment were placed, the microplate was incubated with constant shaking. after the time in which the optical density was determined at time 0, then every half hour for 24 h at 37°C and the percentage inhibition was determined by percentage calculations. Measurements were carried out, at a wavelength of 570 nm in triplicate. All data were analyzed by IBM SPSS Statistics 25 and are expressed as mean values $\pm$ SE. Statistical analyzes were carried out using ANOVA and Tukey's multiple comparison test. A *P* value ≤ 0.05 was considered statistically significant.

Results and Discussion

Synthesis of Alumina Spheres

The alumina spheres were obtained by the method using ion encapsulation agent by encapsulating the sodium alginate and PVA as a binder. A mixture of α-alumina, deionized water, sodium alginate and PVA was performed. With this mixture 4.38 ± 0.31 green spheres were obtained 4.65 mm ± 0.30 mm in width and height with a sphericity of 0.94 ± 0.07 as shown
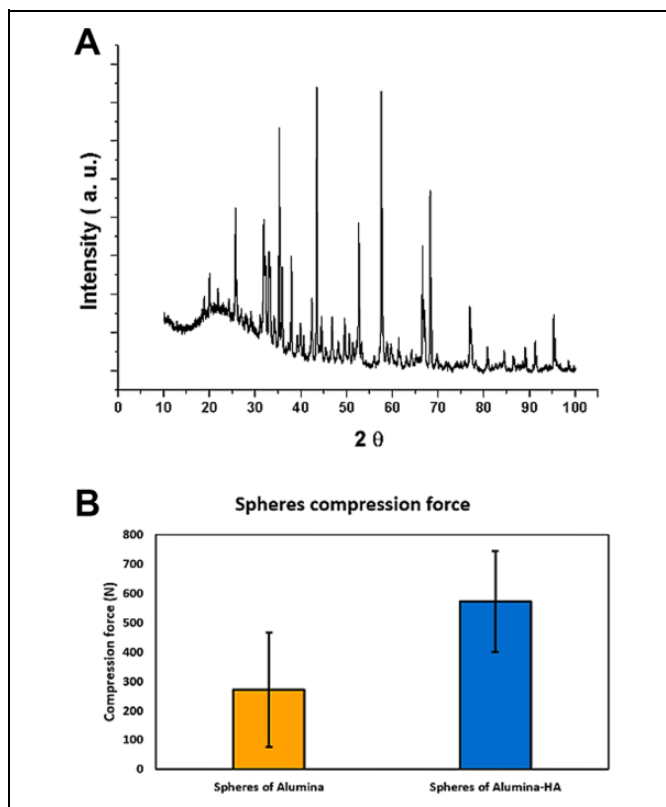

Figure 4. (A) XRD pattern of alumina-hydroxyapatite sphere and (B) compression force analysis for alumina and alumina-hydroxyapatite composites.

in Figure 1A by normal camara. In Figure 1B, sintered alumina sphere is present in digital microscope, the sintered alumina spheres presented an irregular porous surface with white coloration and the structure exhibit high mechanical strength according to previous results, with a shrinkage of around 12%. Before the heat treatment, the spheres showed round, rectangular and square particles, which are the characteristic shapes of the powders used as raw material, with diameters of 0.5 to 1 μm. After sintering, the spheres presented an interlocking and grain-growing structure, with particles with the largest size of around 2 μm according SEM image in Figure 1C. The sintering process helped to decrease the porosity and strength of the spheres. In Figure 1D the characteristic crystal planes of the α-alumina phase are observed according to the JCPDS card 10-0173. The high crystallinity and purity of the alumina spheres obtained according to the DRX and EDX results is remarkable (Figure 1E). In Figure 1F, the heat-treated spheres at 1600°C show strong and well-defined bands in the infrared spectrum for Al-O bonds according to an α-alumina crystal structure according to the DRX results. This phase is demonstrated by the well-defined peaks at 25°, 35°, 37.5°, 43°, 52°, 57°, 61.5°, 66°, and 68°, which correspond to (012), (104), (110), (113), (024), (116), (018), (214) and (300) crystalline planes, according to JCPDS File no. 10-0173 crystallographic card, by evaluation of the Scherer formula for the crystal of
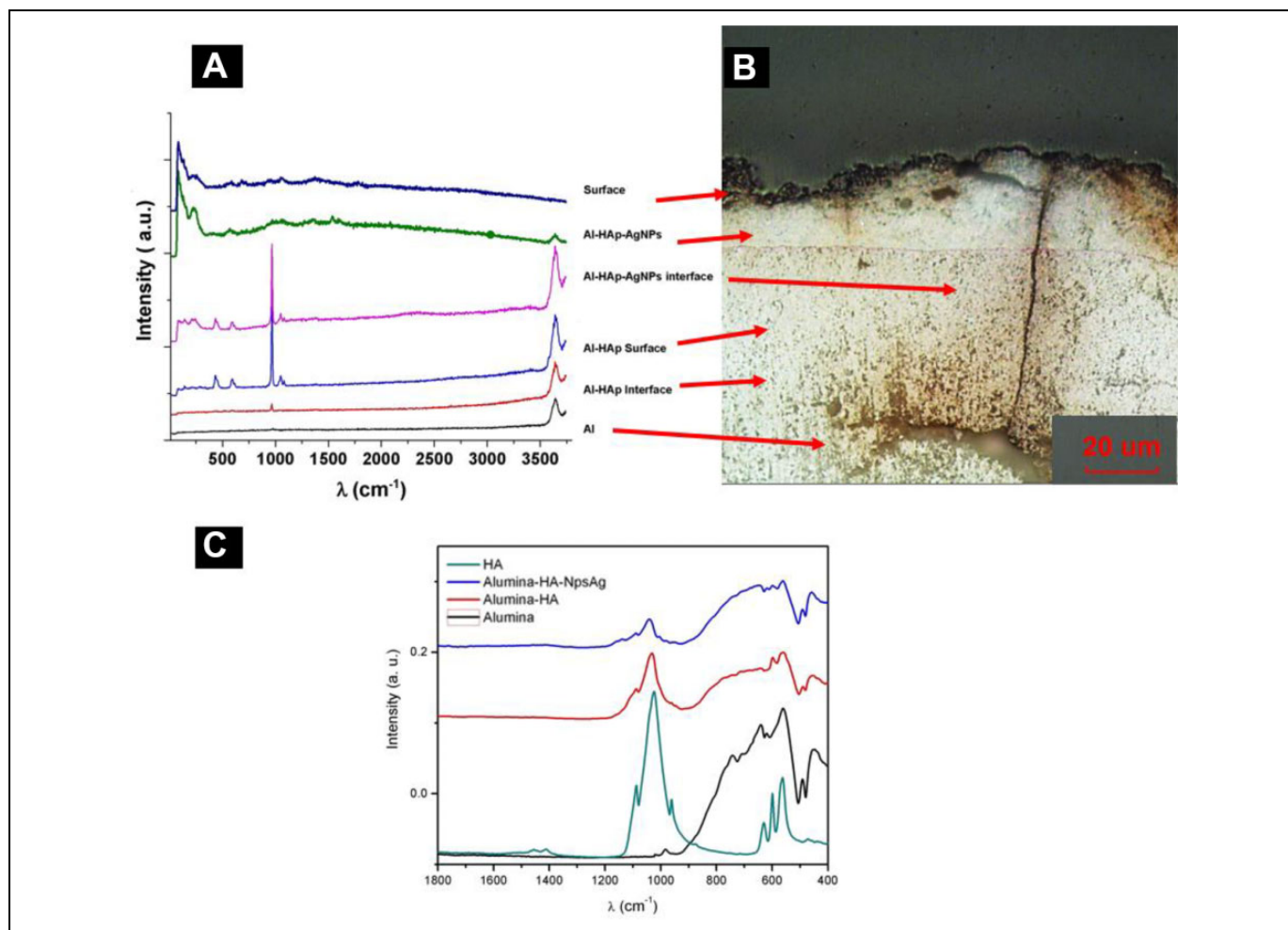
Figure 5. (A) Raman spectra, (B) digital micrograph image and (C) infrared spectra of spheres.

alumina the size are 124 ± 3.8 nm. In the case of a corundum crystalline structure, it is composed of only octahedral AlO_6 with strong characteristic bands near 635, 567 and 496 cm^{-1}, along with some other bands of lower intensity around 450 and 780 cm^{-1}. The IR spectrum for alumina sphere shows characteristic bands at 438, 493, 585 and 642 cm^{-1}; with the appearance of another strong bands near 635, 565 and 491 cm^{-1}, together with some other bands of less intensity around 450 and 413 cm^{-1}. This arrangement of aluminum atoms and oxygen denotes the formation of α-Al_2O_3. Furthermore, no bands belonging to the precursors used to obtain the alumina spheres are observed.

The silver nanoparticles were synthesized by chemical reduction, using this method a slightly viscous reddish-brown solution was obtained which, when diluted, turned yellow. The particle size was determined by dynamic light scattering, which had a size of 5.6 ± 2.9 nm, also the particles exhibit a zeta potential of -55 ± 3.4 mV, indicating that they have good stability. The micrographs by transmission electron microscopy (TEM) of silver nanoparticles confirmed a spherical morphology with no agglomeration and diameters between 5 to 10 nm. The UV-Vis spectrum of AgNPs provided an absorbance peak at 410 nm pronounced for surface plasmon resonance (SPR) of silver nanoparticles with sizes of 5 to 20 nm, supporting the results of DLS in accordance with previously reported data.[27]

Scanning electron microscope micrographs of the half-cut alumina-HAp spheres are shown in Figure 2. In micrograph A and B 2 phases are observed with the backscattered electron detector, the central one of the alumina and the peripheral one, made up of the flake-shaped HAp crystals. Figure 3 shows the mapping of the alumina-hydroxyapatite spheres. In this figure the elemental distribution observed in the sample are calcium, phosphorus, aluminum, oxygen, and carbon. Calcium and phosphorus are found on the periphery of the sphere, indicating that it is the part of the coating, while aluminum and oxygen are found in the core of the sphere formed by alumina. The mapping shows a good delimitation of the distribution of calcium, phosphorus, and aluminum. Needle and plate hydroxyapatite crystals appear at low synthesis temperatures which indicates temperature was uniform in the formation of crystals.

Uniform HAp distribution into the alumina ceramic matrix is a prerequisite for producing high quality *Al-HAp* reinforced composite, HAp particles were uniformly attached onto the
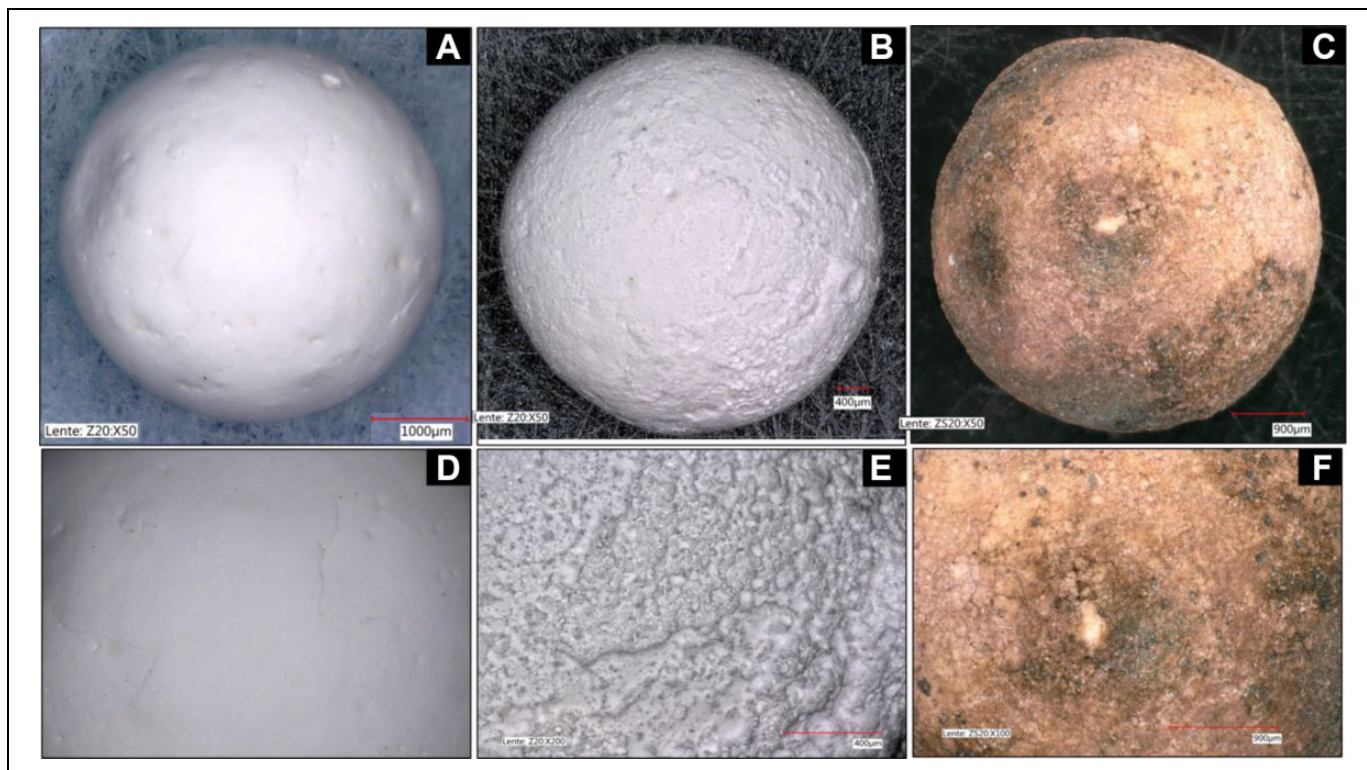
Figure 6. Digital microscope photographs, Al spheres (A) 50× and (D) 100×, Al-HAp spheres (B) 50× and (E) 200× and the Al-HAp-Ag spheres (C) 50× and (F) 100×.

surfaces by Sol-Gel process, as indicated in the microstructural analysis. The crystalline phases of the spheres were investigated using XRD (Figure 4A). XRD patterns show α-alumina and additional peaks that belong to HAp which are located at 26.12°, 32.1°, 33.3°, 39.9°, 47.1° and 49.5°, which belong to the planes (002), (211), (202), (310), (312) and (321), respectively. The XRD patterns of HAp agree with the standard of hydroxyapatite phase JCPDS no.00-009-0432. The crystal size for HAp is 38.3 ± 1.5 nm. Sintering process certainly improved material diffusion, in this case that final composite could be consolidated at low temperature. The principal advantages are the short sintering cycles without microstructure changes and damage of sphere structure according to Figures 2 and 3. The presence of HAp in the composite reveals strong adhesion with alumina matrix, as manifested by increase in mechanical properties in Figure 4. It seems that resistance to compression force leave a composite with double module of Young, for Al spheres is 272 ± 195 N and Al-HAp has 573 ± 172 N. A considerable increase of the properties is associated significant energy dissipation for the presence of HAp crystals in the surface. Therefore, the Al-HAp composite demonstrated an increase in the value by 210% as compared to Al sphere.

Raman spectrum of the alumina, alumina-HA, alumina-HA-Ag and HAp spheres is shown in Figure 5A. Raman for alumina spectra shows bands at 1360 and 1390 cm^{-1} for α-Al$_2$O$_3$ because laser of 532 nm doesn't activate the polarizability during the vibration resulting in no bands in the spectra. For a vibrational transition to be Raman active, the molecule must

undergo a change in polarization.[28,29] A pronounced band at 3635 cm^{-1} due to the hydroxyl groups of HAp is notable in the alumina spectrum, this band increases when the HAp cover increases and decreases in areas where the amount of HAp is less. The Raman spectrum of the HAp presented principal bands at 437, 587, 961, 1046 and 1079 cm^{-1}, the band at 961 cm^{-1} being the most intense as seen in Figure 5A, When the sphere is coated with hydroxyapatite the existence of the principal band at 961 cm^{-1} in the spectra occur, the band at 961 cm^{-1} remains noticeable and increases at higher presence of HAp, the bands located at 437 and 587 cm^{-1} are attributed to the flexural modes of the phosphate group, the 961 cm^{-1} band is a typical phosphate band associated with carbonated apatite and it is assigned to the presence of acid phosphate coming from the tricalcium phosphate, while the 1046 and 1079 cm^{-1} bands are related with the vibration modes of stretching of the phosphate group. It has registered a degenerated asymmetric stretching (v3) vibrational mode of the phosphate group at 1090 cm^{-1} and bending mode (v4) for phosphate, normally found at 578 cm^{-1} for pure hydroxyapatite.[30] According to Raman and infrared spectroscopy analysis, the presence of phosphate groups in the synthesized hydroxyapatite is confirmed, without the presence of bands corresponding to another phase. An increment in the Raman intensity of HAp bands is observed when AgNPs is absorbed, for the contribution generated by AgNPs. It has been reported that noble metals can display a scattering enhanced in Raman spectroscopy.[31] The micrograph in Figure 5B shows the presence of 3 phases in the
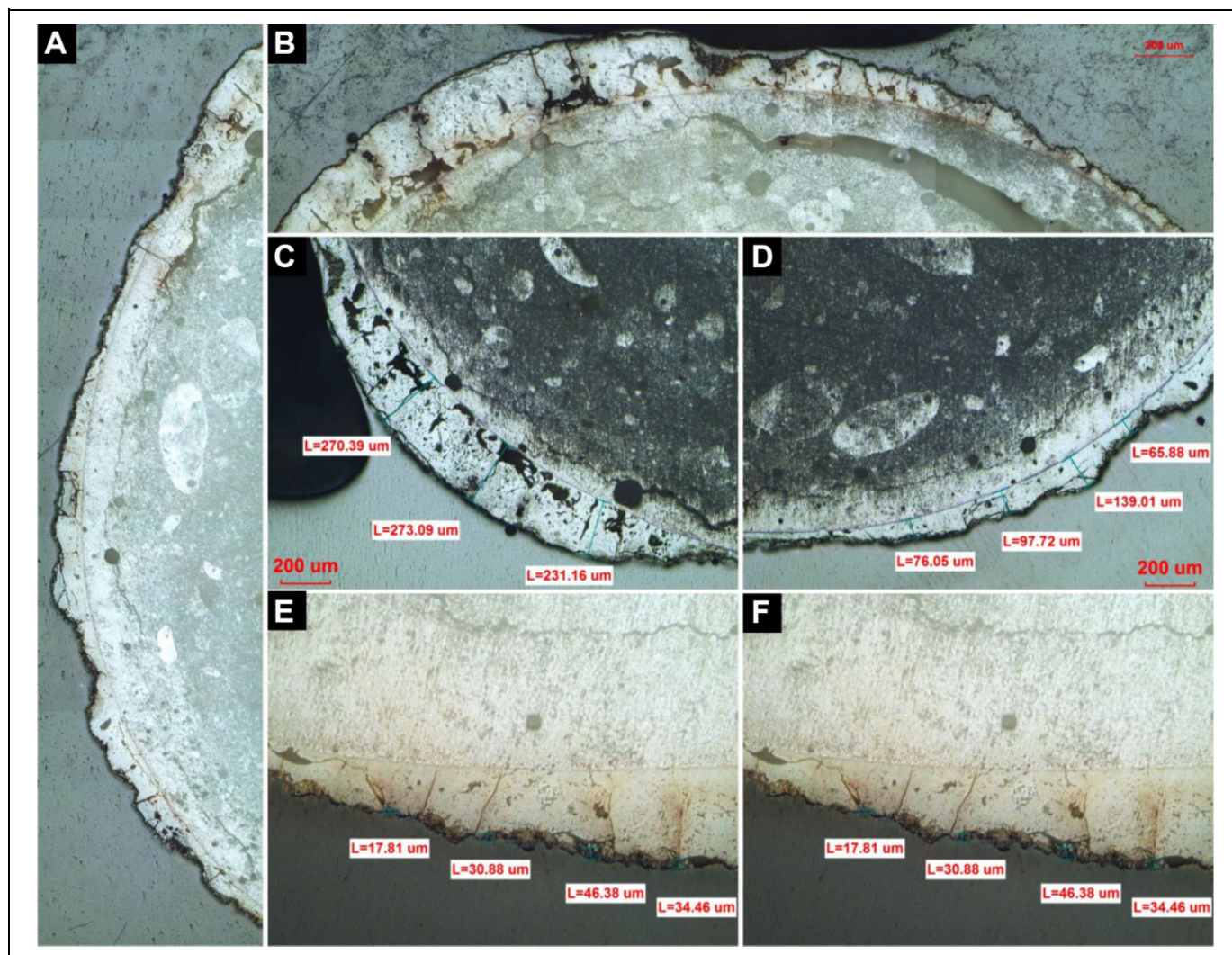
Figure 7. Al-HAp-Ag spheres by metallographic microscope, (A) and (B) assembly of spheres at 100×, (C) and (D) thickness mediation of hydroxyapatite at 100×, (E) and (F) thickness measurement of silver nanoparticles at 200×.

spheres, the first phase (external part of the sphere) is brownish-yellow with bright spots, the second phase (intermediate part) is white with the presence of brown cracks. The yellow and the third phase (internal part) is light yellow and has a smooth morphology with the presence of some pores. HAp exhibits a great affinity for the AgNPs which is shown by the adsorption process that was carried out onto the HAp surface. It is remarkable in light microscopy image of brown spots due to the adsorption of silver and these areas increase in dark color tones when HAp is covered due to increased adsorption. It is also visible as right through the cracks and pores adsorption of silver occurs.

The infrared spectrum of the alumina, alumina-HAp, alumina-HAp-Ag and HAp spheres is shown in Figure 5C. The IR spectrum shows in the case of alumina (black spectrum) a wide band between 585 and 875 cm^{-1} and characteristic bands at 438, 493, 585 and 642 cm^{-1}. A broadband between 500 and 1000 cm^{-1} corresponds to coordinated O-Al-O bonds. The appearance of 2 strong bands near 635, 565 and 491 cm^{-1} along with some other bands of less intensity around 450 cm^{-1} denote the arrangement of aluminum and oxygen atoms of α-Al$_2$O$_3$. No bands belonging to the precursors used to obtain the alumina spheres are observed. In the IR spectrum of alumina-HAp (aqua blue spectrum) 2 bands are observed at 446 and 492 cm^{-1} and a broadening from 900 to 638 cm^{-1} corresponding to the O-Al-O bonds of the alumina, 3 bands at 568, 595 and 638 cm^{-1} and 3 other bands at 1094, 1036 and 1005 cm^{-1} corresponding to the P-O bonds of the hydroxyapatite. It should be noted that no additional phase was formed in the process of HAp shell formation on the alumina surface. In the IR spectrum of alumina-HAp-Ag (blue spectrum) no differences are observed on the sphere, thus indicating no chemical modification of the structure of HAp or alumina occurs, therefore, a physical adsorption process of silver in the HAp follows.[27] Al-HAp spheres were doped with silver nanoparticles, the AgNPs adhered to the surface of the Al-HA spheres by simple adsorption as can be seen later in the micrographs of the spheres. The Al-HAp spheres were immersed in the AgNPs solutions for 72 h, after 72 h, they were
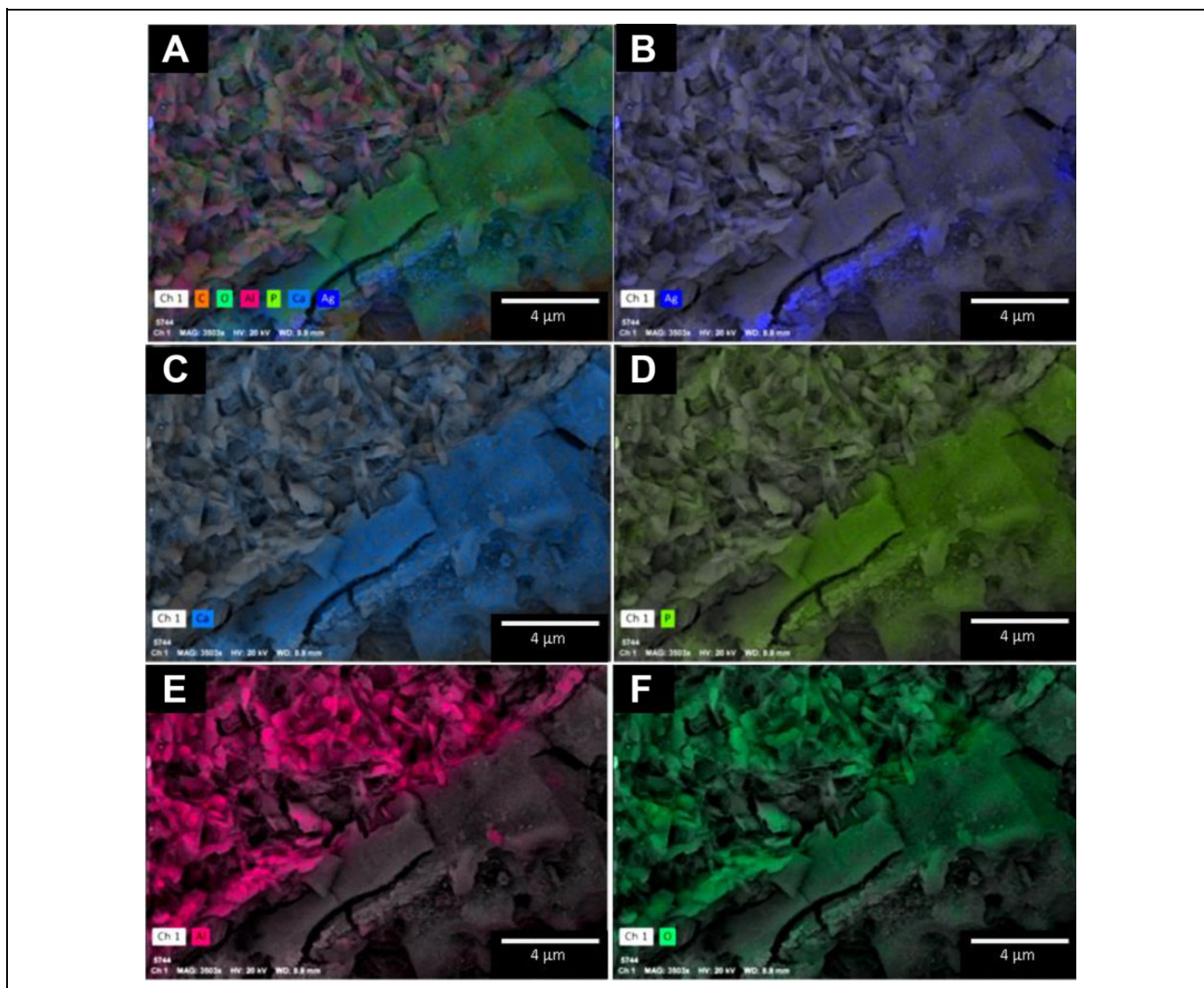
Figure 8. Compositional analysis Al-HAp- AgNPs SEM, (A) carbon, oxygen, phosphorus, calcium, carbon and silver, (B) silver, (C) calcium, (D) phosphorus, (E) aluminum and (F) oxygen.

removed from the solution and subjected to drying at 100°C for 24 h and afterwards at 200°C for 3 h. The Al-HAp spheres changed from a white color to a dark brown color when immersed in the AgNPs solution. Figure 6 shows the Al spheres (A and D), Al-HAp spheres (B and E) and the Al-HAp-Ag spheres (C and F) by digital microscopy with the objective of 50 and 100×. The alumina sphere is observed smooth and uniform with the presence of pores, the hydroxyapatite-coated alumina sphere is observed with porosity. The sphere doped with silver nanoparticles is observed with color variation from yellow to dark brown.

Figure 7 shows the Al-HAp-Ag spheres by metallographic microscopy. In Figure 7A and B the presence of 3 phases can be observed, the first phase of brown color located on the periphery of the sphere and in minimal presence, the second light-colored layer of variable diameter throughout the sphere with the

presence of yellow-brown colored cracks for hydroxyapatite, and the third phase a little more opaque than the second phase corresponding to the alumina core. The HAp second phase is well delimited by the third Al phase as seen in the micrograph, clearly it shows a line between the 2 phases. Figure 7C and D shows an amplification of the surface of hydroxyapatite, their thickness can be seen from 70 to 273 μm. Figure 7E and F shows the adsorption of silver by brown contour.

Figure 8 shows the elemental distribution mapping where the distribution of aluminum, oxygen, calcium, phosphorus, and silver can be observed. In this micrograph it can be observed that the inside of the sphere is composed of aluminum and oxygen, due to the presence of alumina in the core of the sphere, with calcium and phosphorus abundant on the outer part due to the covering with hydroxyapatite, while silver is on the surface of the sphere adhered to hydroxyapatite. In linear
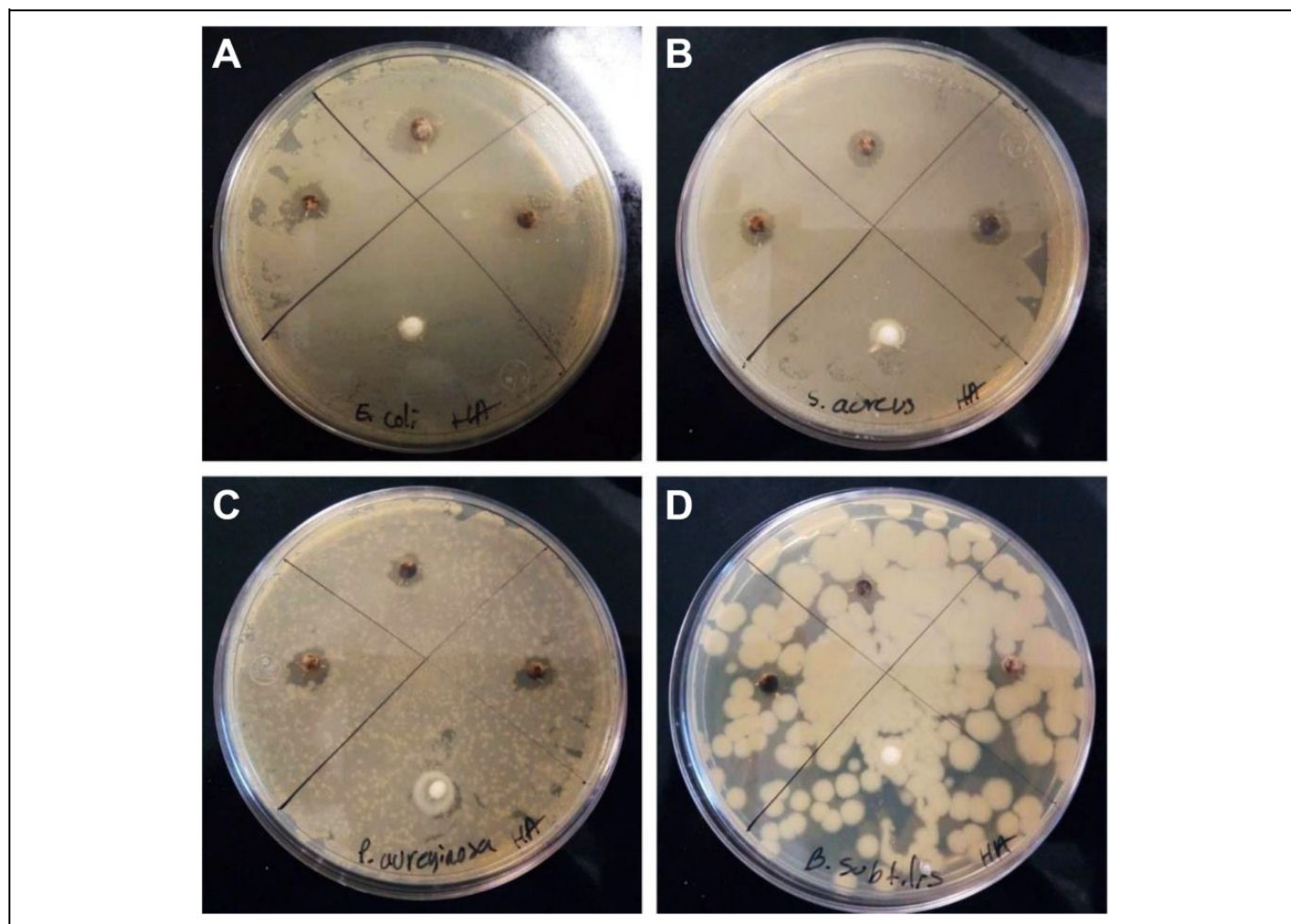
Figure 9. Inhibition halos for: (A) *Escherichia coli*, (B) *Staphylococcus aureus*, (C) *Pseudomonas aeruginosa* and (D) *Bacillus subtilis*.
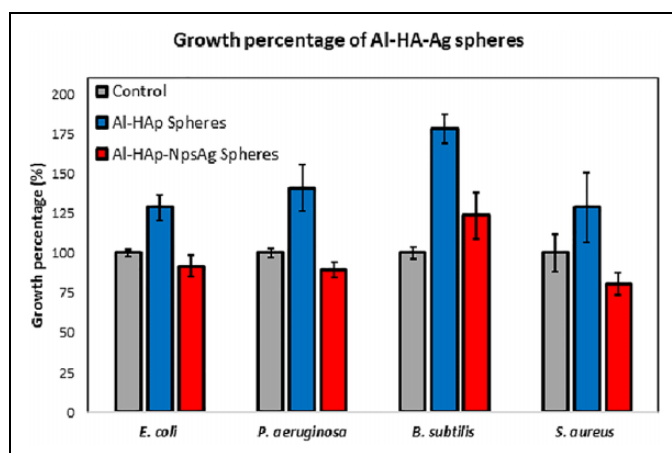

Figure 10. Growth percentage of Al-HAp-AgNps spheres.

scan from the center to the surface of the sphere, the presence of aluminum decreases, calcium and phosphorus increases due to coating process and silver is the only element on the surface.

Antibacterial Activity

The bacterial sensitivity of Al-HAp-AgNPs spheres was determined by disk diffusion method, from which the inhibition zone in mm was obtained for 4 bacteria, 2 Gram-negative (*E. coli* and *P. aeruginosa*) and 2 Gram-positive (*S. aureus* and *B. subtilis*) were tested. The assay was performed in triplicate and used as negative control spheres of Al-HAp. The disk diffusion method demonstrated the sensitivity of bacteria to Al-HAp-Ag spheres. Three bacteria showed sensitivity to Al-HAp-Ag spheres. In Figure 9 the inhibition halos formed by each bacterium are reported as follows. (A) *E. coli* present an inhibition of 8.88 $\pm$ 1.42 mm, (B) *S. aureus* present an inhibition of 7.67 $\pm$ 0.48 mm, (C) *P. aeruginosa* obtained an inhibition of 7.91 $\pm$ 0.7 mm, while (D) *B. subtilis* do not show susceptibility to Al-HAp-Ag spheres.

The antibacterial effect is also determined by the method of turbidimetry and the percentage inhibition for each bacterium used was obtained. In Figure 10 it is observed that the bacteria with increased susceptibility to Al-HAp-Ag spheres was *S. aureus* with a percentage inhibition of 20%, followed by *P.*
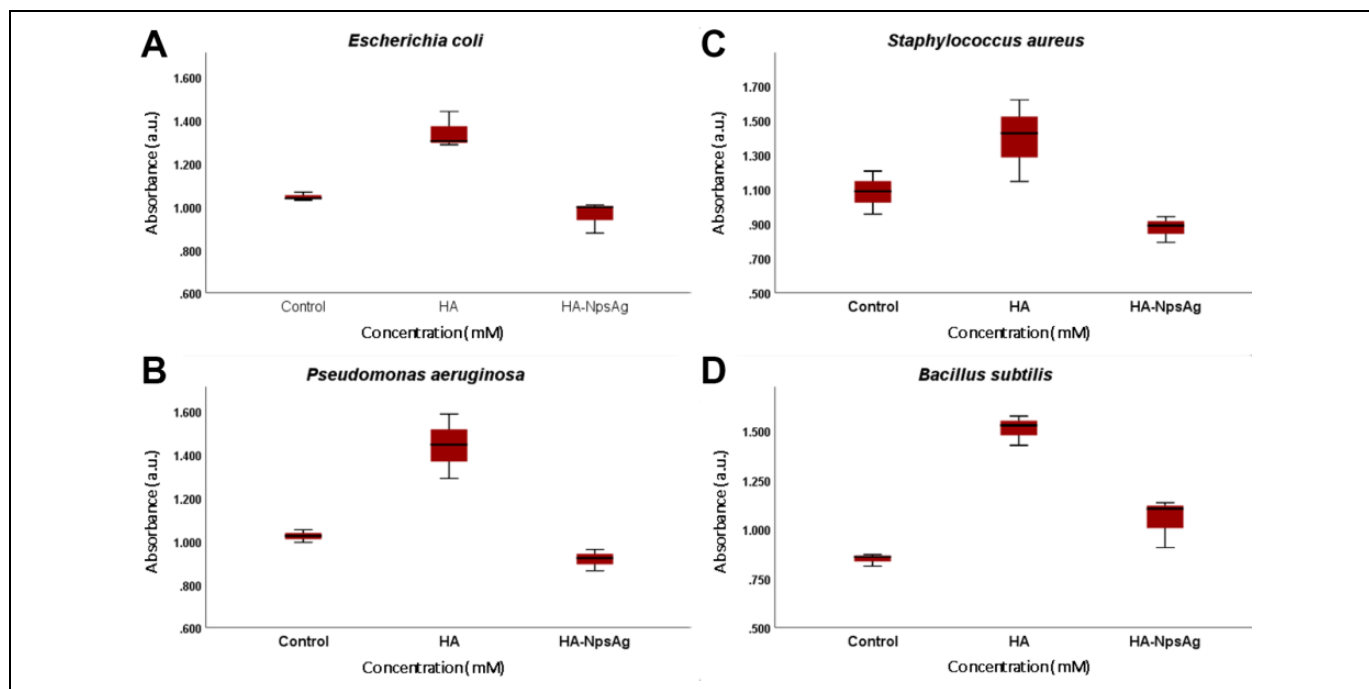
Figure 11. Box plot of the inhibition of Al-HAp-Ag spheres.

aeruginosa and *E. coli* with a percentage of inhibition of 11% and 9% respectively, while *B. subtilis* obtained a growth of 123%, indicating that it was not susceptible to Al-HAp-Ag spheres. One can also observe that the hydroxyapatite induces growth in bacteria because of observed higher growth rate, this phenomenon is observed in all the bacteria that was employed.

Through analysis of variance via Tukey with a significance level of 0.05 and using the absorbance obtained as response variable, it is observed that there is a significant difference between control and treatment for all bacteria, therefore, there is a significant inhibition for *E. coli, P. aeruginosa* and *S. aureus* as can be seen in Figure 11.

By extrapolating the previously reported results for HA-Ag composites.[30] with the Al-HAp-AgNPs spheres, a greater inhibition was observed at a lower concentration by the powders, this is due to the greater diffusion that the silver particles present when found in a free medium, compared to the spheres, the silver particles adhered more to the surface of the sphere, so its release is minimal, which translates into a lower antibacterial effect, which could be used for a prolonged release of silver ions in dental prostheses. The higher adhesion of the silver particles in the spheres is mainly due to repeated heat treatment in the spheres to have a greater sintering of the hydroxyapatite on the surface, which causes the HAp structure to retain more strongly the silver nanoparticles. The literature mentioned that the hydroxyapatite adsorption mechanism is based on ion exchange transport with exchangeable cations such as Ca^{2+} and H^+. Therefore, the greater the thermal treatment of hydroxyapatite, the greater the crystallization of HAp that occurs, which means a greater ion exchange and retention of the silver

cation. According to the results of the hydroxyapatite coating on the spheres, it occurs due to the loss of water and hydroxyl groups with heat treatment, causing a more crystalline surface of HAp; therefore, by putting the spheres into silver adsorption the HA structure changes from the flaky shape to a smooth and spongy surface according to SEM micrographs, causing the exchange of both hydroxyl and the exchange of the strongest Ag^+ cation on the surface of the sphere.

According to the needs of the organisms, metals can be classified as trace elements and xenobiotics, the former includes all those elements which are necessary (in trace concentrations) for cellular processes forming part of enzymes and co-enzymes involved in reactions involving chemicals within an organism while the latter do not have a physiological function in living organisms.[31-33] Silver is a xenobiotic metal found in low concentrations (<2.3 μg/L) in the human body due to its exposure from various sources.[34] The use of silver as a broad-spectrum antibacterial agent is limited by the toxicity of its Ag^+ ions in humans.[35] However, making use of nanotechnology, silver nanoparticles (AgNPs) can be obtained with less toxicity than Ag^+ ions. A study carried out in 2009 by Foldbjerg et al showed that silver ions are more toxic than silver nanoparticles for THP-1 monocytes, obtaining an EC_{50} (maximum mean effective concentration) of 0.624 $\pm$ 0.053 μg/mL in the case of silver ions and 2,436 $\pm$ 0.170 μg/mL for silver nanoparticles.[36] Ag^+ ions are found in low concentrations due to the formation of complexes with various ligands present in natural water and/or body fluids, some ligands such as chlorides, sulfides, thiosulfates and organic compounds can mitigate the toxicity of silver ions.[37,38] Zhang

et al determined that AgCl is less cytotoxic than silver ions when exposed to red blood cells and human mesenchymal stem cells (hMSCs).[39] As it has been reported that the toxicity of silver nanoparticles is related to their size, shape, reactivity and release capacity, hence the importance of having a suitable release medium.[35,40] Rajasekharreddy and Usha in 2014 determined the cytotoxicity of silver nanoparticles obtained from silver nitrate and hexane extract of *S. foetida*, the MTT tests and DNA fragmentation in HeLa cells was determined and it was reported that the nanoparticles synthesized with a concentration of 16 mg/mL showed no toxicity or DNA fragmentation.[41]

It is necessary to find a balance between the antibacterial capacity of a material and its toxicity to human cells, so an antibacterial agent should not be active unless it is in contact with the microorganism to be eliminated. Loher et al synthesized a material based on calcium phosphate (TPC) with silver nanoparticles, obtaining a 97% reduction in CFU, while the pure TPC material presented an increase in bacterial concentration by 10 times due to the supply of ions. specific (Ca^{2+} and PO_4^{3-}), thus demonstrating that by containing silver nanoparticles in a matrix that contains trace elements necessary for bacterial growth, silver is released from the matrix by the action of bacteria when extracting trace elements.[42] By having the silver nanoparticles on the surface of the Al-HAp sphere, we have modified their biological activity and prevent their release into the environment. Having metal ions in various materials allows for localized, non-cytotoxic antibacterial activity at low concentrations.[41]

Conclusion

Alumina spheres were obtained by the method of encapsulation, which were coated with hydroxyapatite by the sol-gel process for the obtention of Al-HAp spheres. Al-HAp spheres were characterized and the presence of 2 phases was identified; the core compound alumina and surface crystalline HAp. The composite reveal sinterability, phase purity and stability and the composite are enhanced in properties by the cover of hydroxyapatite. The crystal size for alumina and hydroxyapatite are around 124 and 39 nm respectably. Al-HAp-Ag spheres was obtained by simple adsorption of AgNPs. The composite is suitable to be processed into porous structure by encapsulation and sol-gel process. The Al-HAp-Ag spheres presented sensitivity in bacteria *E. coli, P. aeruginosa* and *S. aureus*, obtaining a maximum inhibition of 20% in *S. aureus*. The degradation of the hydroxyapatite matrix by microorganisms causes the release of silver nanoparticles and increases their bactericidal effect, having a slow and prolonged release.

Authors' Note

Reyes-López generated ideas, Silva-Holguín and Reyes-López designed experiments, performed the experimental work, Silva-Holguín characterized the materials and devices analyzed results, supervised the entire research work, and Silva-Holguín and Reyes-

ORCID iD

Simón Yobanny Reyes-López 🔟 https://orcid.org/0000-0002-9017-3233

References

1. Esparza JL, Espinosa-Cristobal LF, Cornejo AD, Reyes-Lopez SY. Antimicrobial activity of silver nanoparticles in polycaprolactone nanofibers against gram-positive and gram-negative bacteria. *Ind Eng Chem Res*. 2016;55(49):12532-12538. doi:10.1021/acs.iecr.6b02300

2. Makvandi P, Wang CY, Zare EN, Borzacchiello A, Niu LN, Tay FR. Metal-based nanomaterials in biomedical applications: antimicrobial activity and cytotoxicity aspects. *Adv Funct Mater*. 2020;30(22):1910021.

3. Maharramov AM, Ramazanov MA, Hasanova UA. Nanostructures for antimicrobial therapy—the modern trends in the treatment of bacterial infections. In: Grumezescu AM, ed. *Antimicrobial Nanoarchitectonics*. Elsevier; 2017:445-473.

4. Ojeda-Garcés JC, García EO, Salas LA. Streptococcus mutans and dental caries. *CES Odontol*. 2013;26(1):44-56.

5. Coll HA, Jiménez MS, Castro NC. Conocimiento de la microbiota de la cavidad oral a través de la metagenómica. *CES Odontol*. 2015;28(2):112-118.

6. Gamboa F, Chaves M. Antimicrobial potential of extracts from *Stevia rebaudiana* leaves against bacteria of importance in dental caries. *Acta Odontol Latinoam*. 2012;25(2):171-175.

7. Sánchez FR. Algunas consideraciones sobre caries dental, fluoruros, su metabolismo y mecanismos de acción. *Acta Odontol Venez*. 2008;46(4):509-516.

8. Vidal JE, Canizález-Román A, Gutiérrez-Jiménez J, Navarro-García F. Patogénesis molecular, epidemiología y diagnóstico de escherichia coli enteropatógena. *Salud Publica Mex*. 2007; 49:376-386.

9. Cantón R, Cobos N, De Gracia J, et al. Tratamiento antimicrobiano frente a la colonización pulmonar por pseudomonas aeruginosa en el paciente con fibrosis quística. *Arch Bronconeumol*. 2005;41:1-25.

10. Bodí M, Garnacho J. Pseudomonas aeruginosa: tratamiento combinado frente a monoterapia. *Med Intensive*. 2007;31(2):83-87.

11. Zendejas-Manzo GS, Avalos-Flores H, Soto-Padilla MY. Microbiología general de *Staphylococcus aureus*: generalidades,

patogenicidad y métodos de identificación. *Rev Biomed*. 2014; 25(3):129-143.

12. Muñoz-Escobar A, Ruíz-Baltazar ÁD, Reyes-López SY. Novel route of synthesis of PCL-CuONPs composites with antimicrobial properties. *Dose Response*. 2019;17(3). doi:10.1177/1559325819 869502

13. Yuan Q, Xu A, Zhang Z, et al. Bioactive silver doped hydroxyapatite composite coatings on metal substrates: synthesis and characterization. *Mater Chem Phys*. 2018;218:130-139. doi:10.1016/j. matchemphys.2018.07.038

14. Tian B, Chen W, Dong Y, et al. Silver nanoparticle-loaded hydroxyapatite coating: structure, antibacterial properties, and capacity for osteogenic induction in vitro. *RSC Adv*. 2016;6(11):8549-8562.

15. Zhang XF, Liu ZG, Shen W, Gurunathan S. Silver nanoparticles: synthesis, characterization, properties, applications, and therapeutic approaches. *Int J Mol Sci*. 2016;17(9):1534.

16. Yun J, Lee DG. Silver nanoparticles: a novel antimicrobial agent. In: Grumezescu AM, ed. *Antimicrobial Nanoarchitectonics: From Synthesis to Applications*. Elsevier; 2017:139-166. doi:10. 1016/B978-0-323-52733-0.00006-9

17. Rus FM, Ramiro GP, García MS, Gómez BR. Cerámicas dentales : clasificación y criterios de seleccion. *Rcoe*. 2007;12(4):253-263. doi:10.4321/S1138-123X2007000300003

18. Thamaraiselvi T, Rajeswari S. Biological evaluation of bioceramic materials—a review. *Trends Biomater Artif Organs*. 2004; 18(1):9-17.

19. Tayyebi S, Mirjalili F, Samadi H, Nemati A. A review of synthesis and properties of hydroxyapatite/alumina nano composite powder. *Chem J*. 2015;5(2):20-28.

20. Raj SV, Rajkumar M, Sundaram NM, Kandaswamy A. Synthesis and characterization of hydroxyapatite/alumina ceramic nanocomposites for biomedical applications. *Bull Mater Sci*. 2018;41(4):93.

21. Ghazanfari SM, Zamanian A. Phase transformation, microstructural and mechanical properties of hydroxyapatite/alumina nanocomposite scaffolds produced by freeze casting. *Ceram Int*. 2013; 39(8):9835-9844.

22. Roque-Ruiz JH, Cabrera-Ontiveros EA, González-García G, Reyes-López SY. Thermal degradation of aluminum formate sol-gel; synthesis of α-alumina and characterization by ^{1}H, ^{13}C and ^{27}Al MAS NMR and XRD spectroscopy. *Results Phys*. 2016;6:1096-1102.

23. Roque-Ruiz JH, Castillo-Ramirez D, Jesús Ruíz-Baltazar AD, Espinosa-Cristobal LF, Reyes-Lopez SY. Preparation of silver-doped alumina spherical beads with antimicrobial properties. *J Nanomater*. 2018;2018:3.

24. Vargas-Martínez N, Ruíz-Baltazar ÁD, Medellín-Castillo NA, Reyes-López SY. Synthesis of α-alumina nano-onions by thermal decomposition of aluminum formate. *J Nanomater*. 2018;2018:2.

25. Santos CJ, Wei TS, Cho B, Kriven WM. A forming technique to produce spherical ceramic beads using sodium alginate as a precursor binder phase. *J Am Ceram Soc*. 2013;96(11):3379-3388.

26. Garibay-Alvarado JA, Espinosa-Cristóbal LF, Reyes-López SY. Fibrous silica-hydroxyapatite composite by electrospinning. *Int J Res Granthaalayah*. 2017;5(2):39-47.

27. Silva-Holguín PN, Reyes-López SY. Synthesis of hydroxyapatite-Ag composite as antimicrobial agent. *Dose Response*. 2020;18(3): 1-14. doi:10.1177/1559325820951342

28. Ayanwale AP, Ruíz-Baltazar AD, Espinoza-Cristóbal L, Reyes-López SY. Bactericidal activity study of ZrO_2-Ag_2O nanoparticles. *Dose Response*. 2020;18(3):6.

29. Reyes-López SY, Acuña RS, López-Juárez R, Rodríguez JS. Analysis of the phase transformation of aluminum formate $Al(O_2CH)_3$ to α-alumina by Raman and infrared spectroscopy. *J Ceram Process Res*. 2013;14(5):627-631.

30. Jesús Ruíz-Baltazar AD, Reyes-López SY, Silva-Holguin PN, Larrañaga D, Estevez M, Perez R. Novel biosynthesis of Ag-hydroxyapatite: structural and spectroscopic characterization. *Results Phys*. 2018;9:593-597. doi:10.1016/j.rinp.2018.03.016

31. Roque-Ruiz JH, Martínez-Máynez H, Zalapa-Garibay MA, Arizmendi-Moraquecho A, Farias R, Reyes-López SY. Surface enhanced Raman spectroscopy in nanofibers mats of SiO_2-TiO_2-Ag. *Results Phys*. 2017;7:2520-2527. doi:10.1016/j.rinp.2017.07.006

32. Jaiswal A, Verma A, Jaiswal P. Detrimental effects of heavy metals in soil, plants, and aquatic ecosystems and in humans. *J Environ Pathol Toxicol Oncol*. 2018;37(3):12.

33. Rey AR, Luna LC, Cantillo GM, Espinosa ME. Efectos nocivos del plomo para la salud del hombre. *Rev Cuba de Investig Biomed*. 2017;35(3):251-271.

34. Lansdown AB. Silver in health care: antimicrobial effects and safety in use. *Curr Probl Dermatol*. 2006;33:17-34.

35. Khan SU, Saleh TA, Wahab A, et al. Nanosilver: new ageless and versatile biomedical therapeutic scaffold. *Int J Nanomed*. 2018;13:733.

36. Foldbjerg R, Olesen P, Hougaard M, Dang DA, Hoffmann HJ, Autrup H. PVP-coated silver nanoparticles and silver ions induce reactive oxygen species, apoptosis and necrosis in THP-1 monocytes. *Toxicol Lett*. 2009;190(2):156-162.

37. Choi O, Deng KK, Kim NJ, Ross L Jr, Surampalli RY, Hu Z. The inhibitory effects of silver nanoparticles, silver ions, and silver chloride colloids on microbial growth. *Water Res*. 2008;42(12): 3066-3074.

38. Boudreau MD, Imam MS, Paredes AM, et al. Differential effects of silver nanoparticles and silver ions on tissue accumulation, distribution, and toxicity in the Sprague Dawley rat following daily oral gavage administration for 13 weeks. *Toxicol Sci*. 2016;150(1):131-160.

39. Zhang S, Du C, Wang Z, Han X, Zhang K, Liu L. Reduced cytotoxicity of silver ions to mammalian cells at high concentration due to the formation of silver chloride. *Toxicol Vitro*. 2013; 27(2):739-744.

40. Chappell MA, Miller LF, George AJ, et al. Simultaneous dispersion–dissolution behavior of concentrated silver nanoparticle suspensions in the presence of model organic solutes. *Chemosphere*. 2011;84(8): 1108-1116. doi:10.1016/j.chemosphere.2011.04.040

41. Radovanovic Z, Jokic B, Veljovic D, et al. Antimicrobial activity and biocompatibility of Ag^+- and Cu^{2+}-doped biphasic hydroxyapatite/α-tricalcium phosphate obtained from hydrothermally synthesized Ag^+- and Cu^{2+}-doped hydroxyapatite. *Appl Surf Sci*. 2014;307:513-519.

42. Loher S, Schneider OD, Maienfisch T, Bokorny S, Stark WJ. Micro-organism-triggered release of silver nanoparticles from biodegradable oxide carriers allows preparation of self-sterilizing polymer surfaces. *Small*. 2008;4(6):824-832.